Li, M., et al., 2018, A dolomitization event at the oceanic chemocline during the Permian-Triassic transition: Geology, https://doi.org/10.1130/G45479.1

## Geological Setting

A total of 22 worldwide sections ranging from the Middle Permian to the Middle Triassic were studied (Fig. DR1), and these sections were arranged into four regional groupings: (1) the East Tethys region (South China Craton), with 10 sections; (2) the South Tethys region (the northern Gondwana margin), with 4 sections; (3) the Middle and West Tethys region, with 5 sections; (4) the Panthalassa region, with 3 sections.

In East Tethys region, 10 sections from the South China Craton with well constrained conodont biostratigraphic zonation (Fig. 2) allow high resolution lithological and sedimentary correlations. At the Permian-Triassic boundary (PTB), Cili, Nhi Tao, Lung Cam and Zuodeng were deposited in shallow subtidal setting (Loope et al., 2013; Luo et al., 2011; Algeo et al., 2007; Wardlaw et al., 2015) that featured the development of a thick-bedded microbialite mainly restricted to the *Hindeodus parvus* zone (Yin et al., 2014). Upwards, the microbialite dominated shallow subtidal environment deepens into inner shallow shelf at the Zuodeng section with water depths of 30~50 m (Yin et al., 2014). The Yangou section spanning from late Changhsingian to the Griesbachian age was deposited in a shallow inner shelf (Tian et al., 2014), and shows distinct features that distinguish it from the shallow subtidal sections, such as the lack of microbialite and oolitic grainstone, indicating a somewhat deeper water depth. The Meishan section, the global stratotype section and point (GSSP) of the PTB (Yin et al., 2001), was located in a deep, offshore setting during the Griesbachian age (Chen et al., 2015). As a transition section from inner

shelf to deep shelf, it comprises of thin bedded marlstone intercalated with calcareous mudstone and lacks microbialite and oolitic limestone. Daxiakou, West Pingdingshan, South Majiashan and Shangsi sections were deposited in the deep shelf/basin setting (Zhao et al., 2007; Li et al., 2007; Wignall and Twitchett, 2002), have a high content of clay, lack microbialite and high energy deposits.

In south Tethys region, Spiti (India), Guryul Ravine (Kashmir), Selong and Tulong sections were located along the Northern margin of Gondwana supercontinent, and have similar lithofacies (Garzanti et al., 1998; Shen et al., 2006) formed on a passive shelf margin. Selong and Spiti were deposited in inner shelf during the Earliest Triassic (Shen et al., 2003; Ghosh et al., 2016) and immediately drowned under the global transgression (Wignall and Newton, 2003). Guryul Ravine and Tulong were deposited in the relative deep shelf setting (Algeo, Hannigan, et al., 2007; Brühwiler et al., 2009) based on their lithology and sedimentary features. High resolution conodont and ammonoid biostratigraphic zonation (Fig. 2) have been established for these sections (Wang et al., 2017; Brühwiler et al., 2009; Bhargava et al., 2004; Orchard and Krystyn, 1998).

The shallow water PTB sections in Middle and West Tethys region show similar lithologies with South China. A typical succession from microbialite in the *Hindeodus parvus* zone to the overlying oolitic limestone is commonly seen (e.g. Balvany (Hungary), Demirtas (Turkey) and Buraydah Quadrangle (Saudi Arabia) (Haas et al., 2007; Loope et al., 2013; Eltom et al., 2018). Such successions are also commonly seen in South China at Cili, Chongyang, and Xiushui (Xie et al., 2007). Another three

sections including Sovetashen (Armenia) and Kurdistan (Iraq) and Zal (Iran) were also deposited in shallow subtidal setting (Alekseev et al., 1983; Tobia and Aqrawi, 2016; Horacek et al., 2007).

In the Panthalassa ocean, the paleoequatorial Kamura section was interpreted to be a shallow marine carbonate formed on a mid-oceanic seamount (Horacek et al., 2009). It spans from the late Changhsingian to the middle Anisian (although the Spathian is absent) (Fig. 2) and provides a long-lasting insight into conditions in the Panthalassa Ocean. On the NW margin of the Pangea close to East Panthalassa, Ursula Creek section deposited in deep shelf/basin setting spanning from the beginning of the Early Triassic to the Middle Triassic (Fig. 2) provides a deep water section on the Panthalassa margin (Wignall and Newton, 2003). The Jesmond section is near the Ursula Creek section but records a shallower setting (peritidal) from the Late Smithian to the Middle Spathian (Sano et al., 2012).

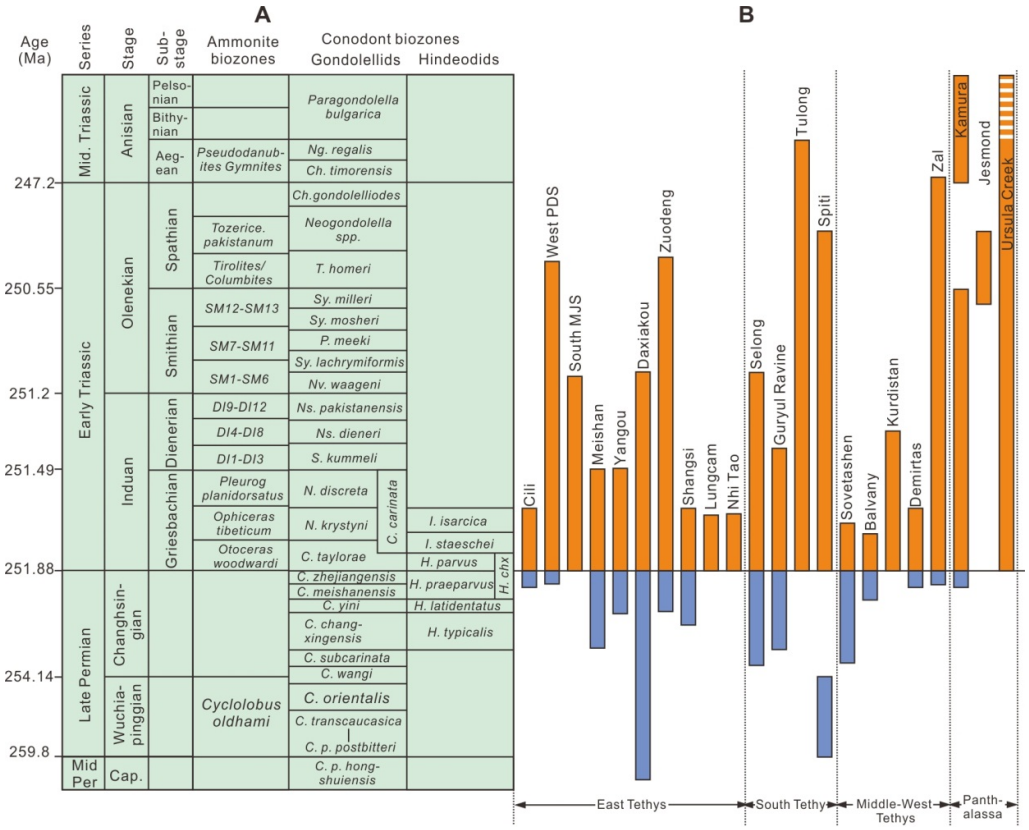


**Figure DR1.** (A) Timescale and biostratigraphic zonation for the Late Permian to the Middle Triassic (modified after Algeo et al., 2013). (B) Stratigraphic ranges of the study sections (white stripes bar indicate the uncertain age). Abbreviation: conodont genera: *C.—Clarkina*, *Ch.—Chiosella, H.—Hindeodus, I.—Isarcicella, M.—Mesogondolella, N.—Neoclarkina, Ns.—Neospathodus, Nv.—Novispathodus, P.—Paulella, S.—Sweetospathodus, Sy.—Scythogondolella, T.—Triassospathodus*. Ammonoid zonation is from Krystyn et al. (2007) and Brühwiler et al. (2010).

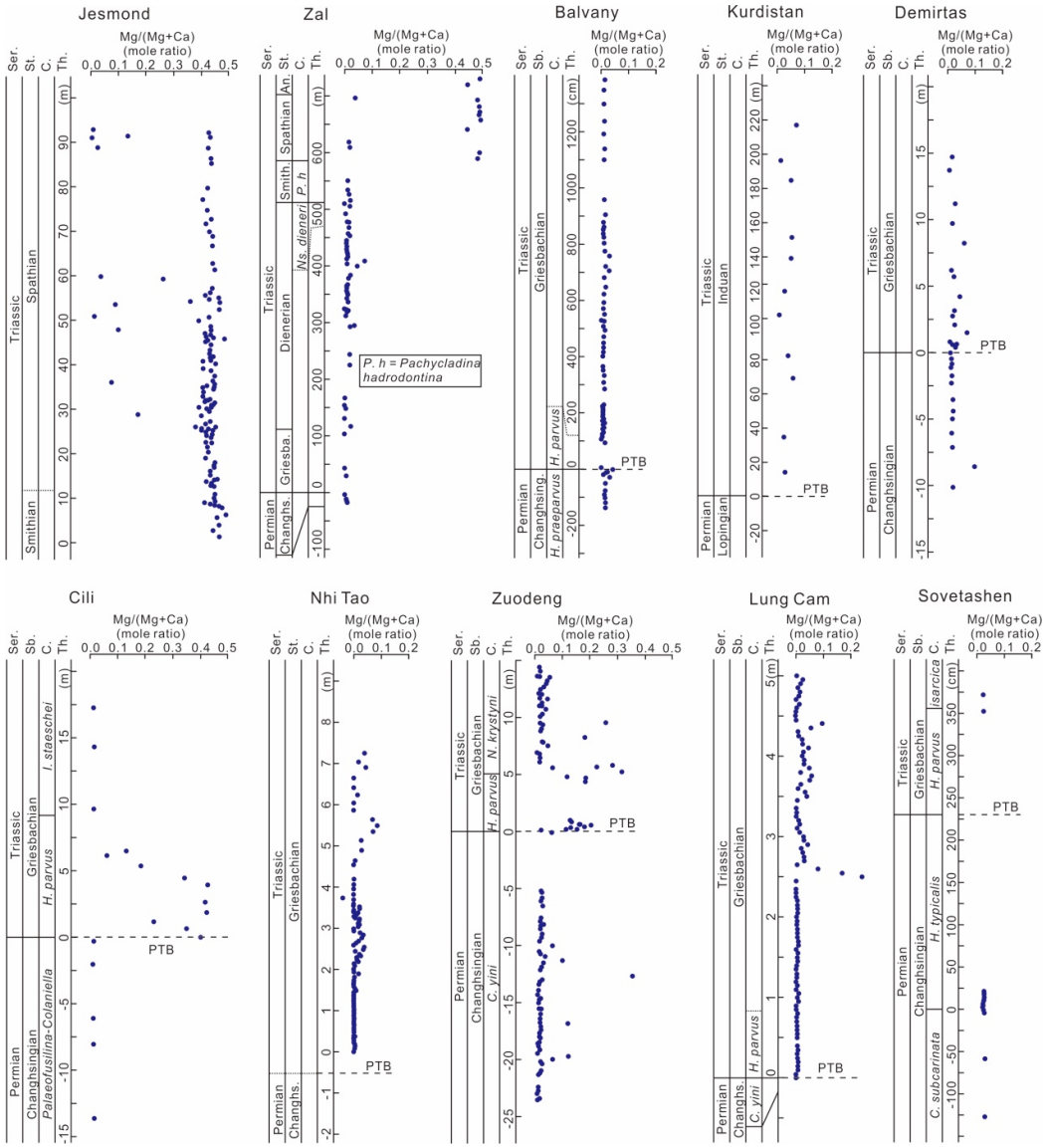


**Figure DR2.** Mg/(Mg+Ca) data for peritidal to shallow shelf sections, high values at the PTB are only seen at Cili and Zuodeng sections. Mg/(Mg+Ca) data of Sovetashen, Kurdistan, Cili and Demirtas is after Alekseev et al. (1983), Tobia and Aqrawi (2016) and Loope et al. (2013), respectively.

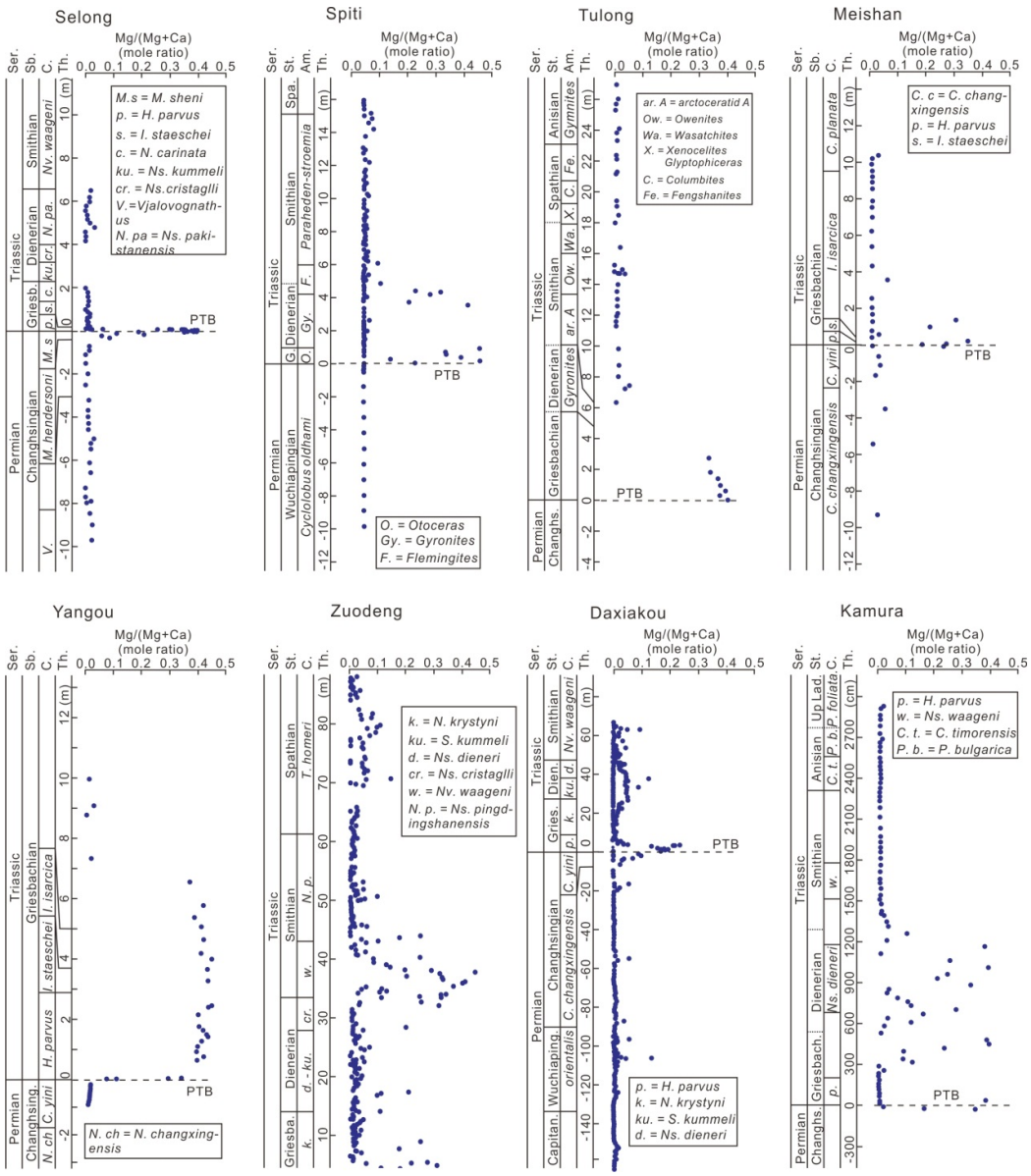


**Figure DR3.** Mg/(Mg+Ca) data for deep shelf to slope sections, an abrupt rise in the Mg/(Mg+Ca) at the PTB is commonly seen for these sections.

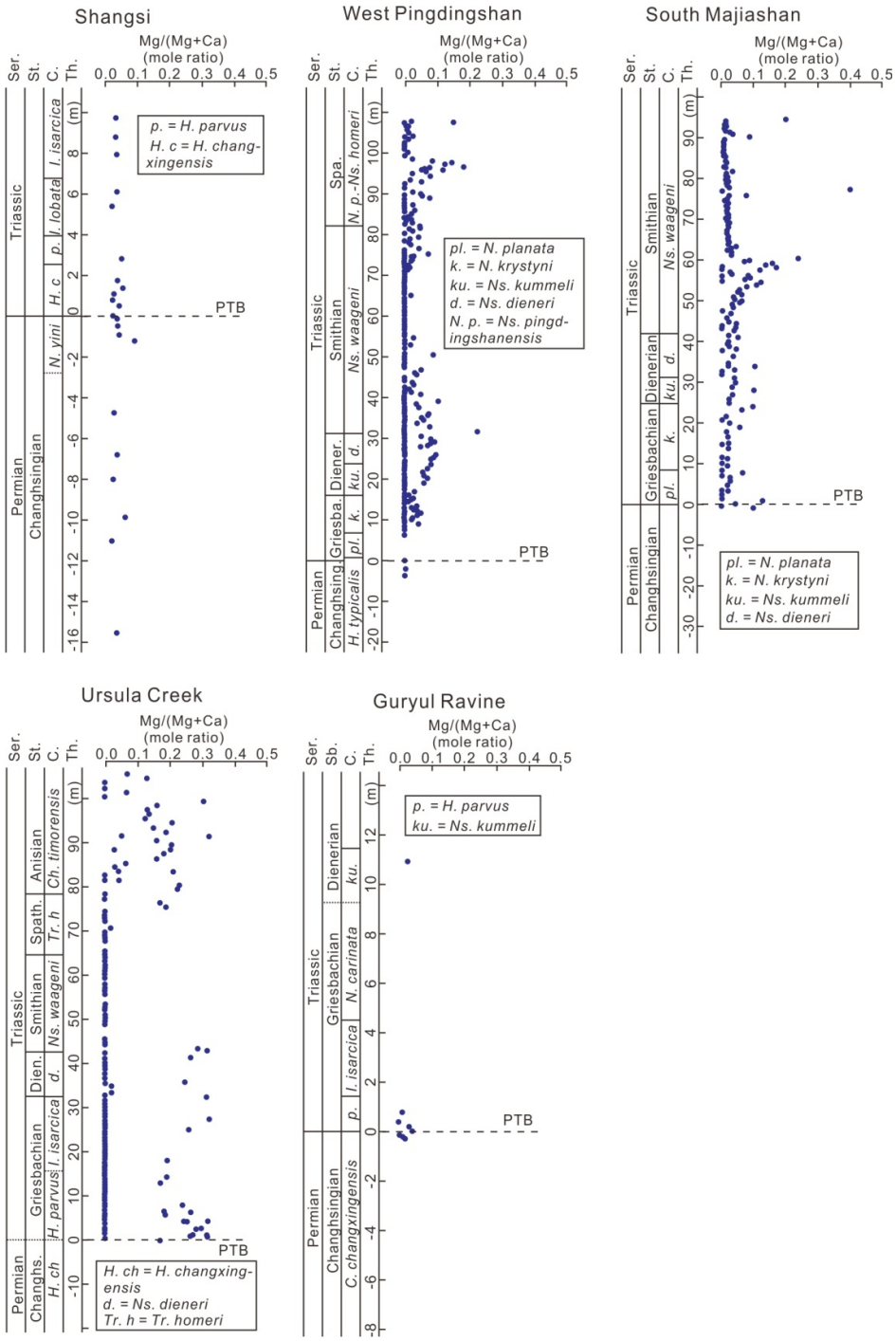


**Figure DR4.** Mg/(Mg+Ca) data for deep shelf and basin sections, an abrupt rise in the Mg/(Mg+Ca) at the PTB is only seen in the deep shelf section Ursula Creek. Notablely, Anisian fluctuations of Mg/(Mg+Ca) ratio at Ursula Creek section are not involved in the calculation of global Mg/(Mg+Ca), this is because samples from the

Anisian Whistler Member at the Ursula Creek consists of abundant calcareous and phosphatic nodules (Henderson, 2011) embedded in thick-bedded shale, which are indicators of strong diagenesis (see Scotchman, 2010).

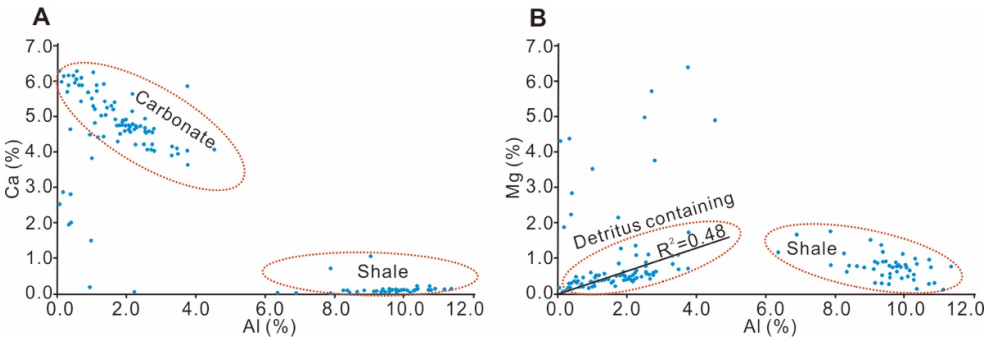


**Figure DR5.** A: Cross-plots of Ca versus Al show carbonate rock is well separated from shale. B: A significant correlation between element Mg and Al in present in detritus-bearing carbonate rock, the detrital fraction of total Mg would be eliminated based on the regression line. Samples are from Spiti (India) section.

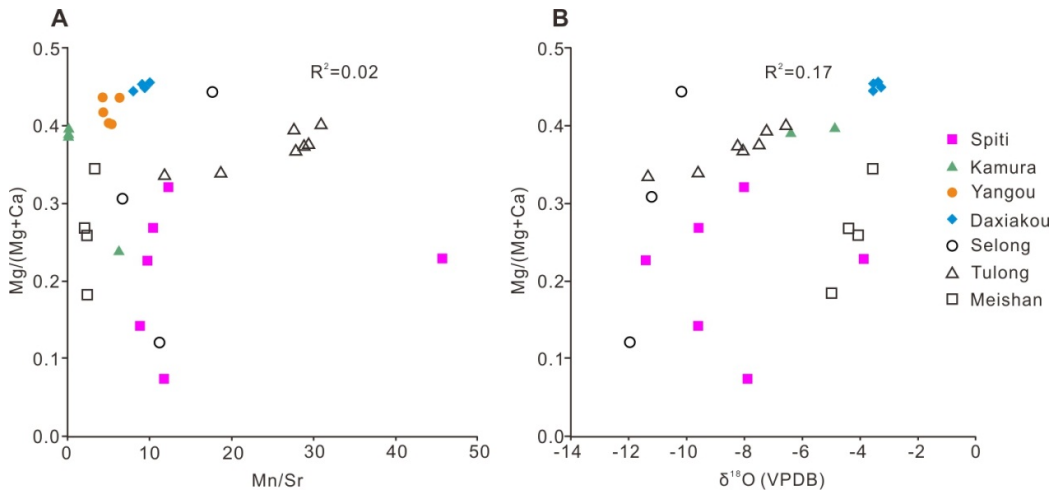


**Figure DR6.** A: Cross-plots of Mn/Sr versus Mg/(Mg+Ca) show non–correlation (n = 33, $R^2 = 0.02$, $p < 0.01$), indicating the dolomite event is not originated from the late burial digenesis. B: $\delta^{18}O$ versus Mg/(Mg+Ca) show a weak positive correlation (n = 26, $R^2 = 0.17$, $p < 0.01$), this trend is in contrast with the one that derived from late diagenetic dolomization.

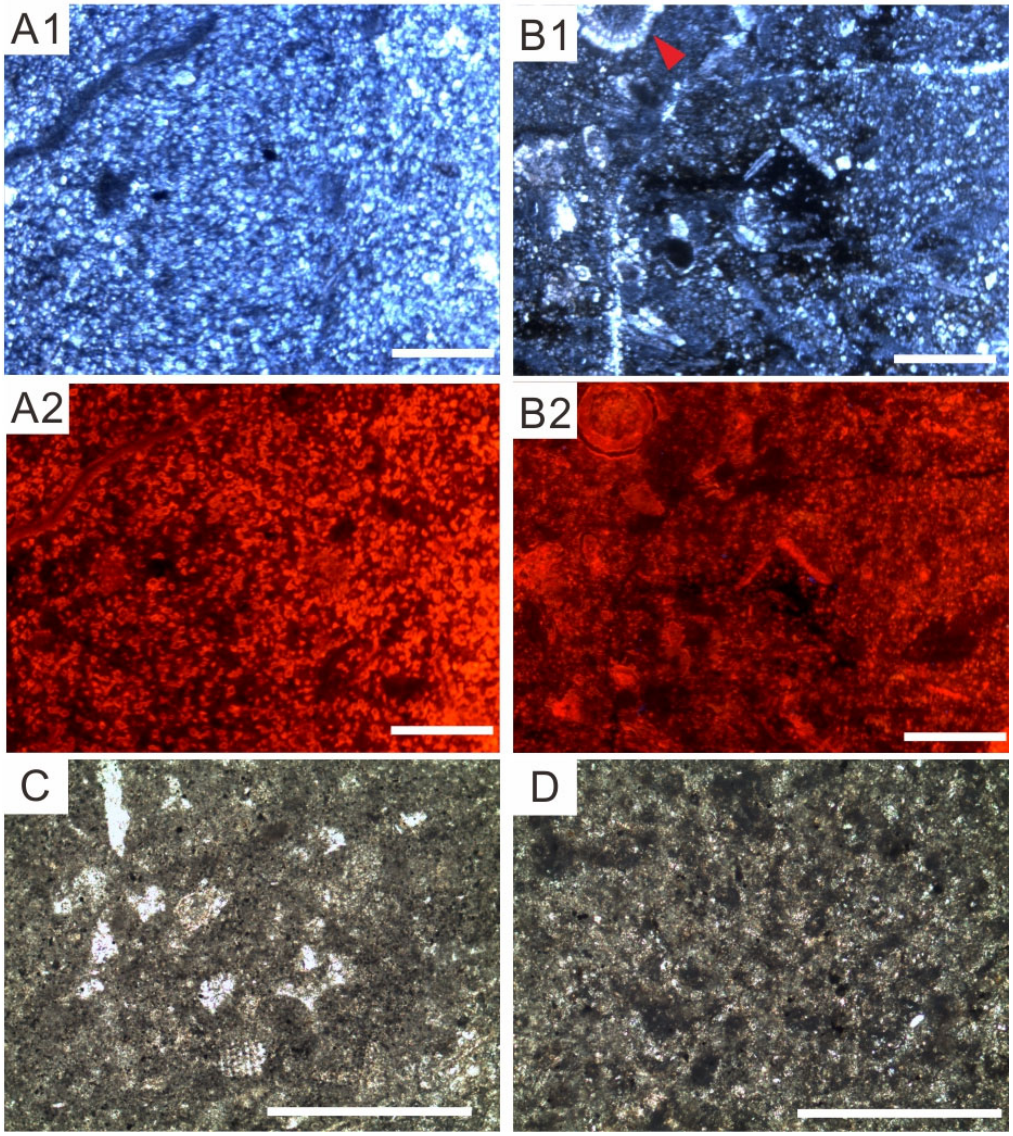


**Figure DR7.** Photomicrographs and CL images of dolomite samples from the PTB sections. A1, A2: Dolostone displays homogenous dolomitic matrix that consists of fine subhedral to euhedral dolomite crystals, note the luminescent dots (A2) are fine dolomite crystals, sample TL2-1.8 from Tulong section, South Tibet. B1, B2: Bioclastic wackestone show occasional bioclastic (red arrow points to a crinoid spine) floating in the dolomitic matrix that consists of fine subhedral to euhedral dolomite crystals (luminescent dots in B2), sample SL-U from Selong section, South Tibet. C, D: Bioclastic wackestone show some bioclastic fragments floating in the dolomitic

matrix that contains abundant dark grey clotted organic matter and pyrites, sample MS-27 from Meishan section, South China.

**Table DR1.** Carbon, oxygen isotope and major element data for the PTB dolostone samples from seven sections.

| Section | Sample | Elevated depth (m) | $\delta^{13}C$ (VPDB) | $\delta^{18}O$ (VPDB) | Sr (ppm) | Mn (ppm) | Mg (%) | Ca (%) |
|---|---|---|---|---|---|---|---|---|
| Spiti | AL2-12 | 0.69 | -2.10 | -11.41 | 478 | 4657 | 2.83 | 13.00 |
| | AL2-11 | 0.58 | -0.28 | -3.85 | 190 | 8692 | 6.35 | 25.56 |
| | AL2-9 | 0.37 | -4.15 | -9.56 | 532 | 5533 | 4.29 | 16.26 |
| | AL2-8 | 0.25 | -4.68 | -7.89 | 550 | 6493 | 2.16 | 30.23 |
| | AL2-7 | 0.11 | -5.74 | -8.01 | 520 | 6372 | 4.35 | 12.61 |
| | AL2-6 | 0.01 | -4.80 | -9.61 | 572 | 5072 | 2.23 | 18.05 |
| Kamura | KAMD-2 | 4.80 | 3.17 | -6.39 | 203 | 23 | 9.99 | 25.73 |
| | KAMD-1 | 4.50 | 3.07 | -4.86 | 237 | 24 | 10.08 | 25.19 |
| | KAMX-23 | 4.20 | | | 145 | 908 | 5.84 | 30.34 |
| | KAMX-7 | 0.40 | | | 213 | 20 | 10.28 | 26.91 |
| Tulong | TL2-0.1 | 0.10 | -1.36 | -6.58 | 234 | 7201 | 8.80 | 21.51 |
| | TL2-0.35 | 0.35 | -2.71 | -8.23 | 204 | 5885 | 7.39 | 19.84 |
| | TL2-0.65 | 0.65 | -1.86 | -7.22 | 205 | 5653 | 7.76 | 19.09 |
| | TL2-1.0 | 1.00 | -1.11 | -7.49 | 169 | 4956 | 7.43 | 19.61 |
| | TL2-1.5 | 1.50 | -1.69 | -8.06 | 164 | 4569 | 7.06 | 19.16 |
| | TL2-1.85 | 1.85 | -2.30 | -9.63 | 199 | 3717 | 6.14 | 18.39 |
| | TL2-2.8 | 2.80 | -2.80 | -11.31 | 254 | 3020 | 5.69 | 17.54 |
| Meishan | MS27-a | 0.05 | 1.27 | -4.88 | 270 | 620 | 4.25 | 18.25 |
| | MS27-b | 0.10 | 1.21 | -5.19 | 300 | 620 | 4.17 | 16.96 |
| | MS27-d | 0.18 | 0.84 | -5.76 | 288 | 697 | 3.14 | 20.57 |
| | MS-29 | 0.30 | 1.39 | -4.34 | 233 | 775 | 5.57 | 16.19 |
| Yangou | LY-27 | 1.45 | | | 106 | 465 | 9.08 | 17.58 |
| | LY-29 | 1.65 | | | 106 | 465 | 8.61 | 15.86 |
| | LY-30 | 1.75 | | | 101 | 542 | 8.30 | 15.09 |
| | LY-33 | 2.10 | | | 109 | 562 | 9.71 | 23.34 |
| | LY35+50 | 3.25 | | | 127 | 807 | 9.46 | 18.76 |
| Daxiakou | XK-11a | 0.05 | 0.76 | -3.55 | 203 | 1627 | 7.95 | 16.58 |
| | XK-11b | 0.13 | 0.89 | -3.31 | 182 | 1704 | 8.08 | 16.44 |
| | XK-11c | 0.18 | 1.07 | -3.52 | 177 | 1627 | 7.61 | 15.34 |
| | XK-11d | 0.25 | 0.97 | -3.36 | 170 | 1704 | 7.66 | 15.28 |
| Selong | S15-U | 0.20 | 2.02 | -10.28 | 305 | 5268 | 8.78 | 18.40 |
| | SL5+16cm | 0.16 | 2.17 | -11.31 | 477 | 3021 | 6.19 | 23.43 |
| | SL5+6cm | 0.06 | 2.66 | -12.06 | 293 | 3176 | 2.22 | 27.01 |

**Table DR2.**

## REFERENCES CITED


Alekseev, A.S., Barsukova, L.D., Kolesov, G.M., Nazarov, M., and Grigoryan, A.G., 1983, The Permian-Triassic Boundary Event: Geochemical investigation of the Transcaucasia section: Lunar & Planetaryence XIV, v. 14, p. 3–4.

Algeo, T.J., Ellwood, B., Nguyen, T.K.T., Rowe, H., and Maynard, J.B., 2007, The Permian-Triassic boundary at Nhi Tao, Vietnam: Evidence for recurrent influx of sulfidic watermasses to a shallow-marine carbonate platform: Palaeogeography, Palaeoclimatology, Palaeoecology, v. 252, p. 304–327, doi: 10.1016/j.palaeo.2006.11.055.

Algeo, T.J., Hannigan, R., Rowe, H., Brookfield, M., Baud, A., Krystyn, L., and Ellwood, B.B., 2007, Sequencing events across the Permian–Triassic boundary, Guryul Ravine (Kashmir, India): Palaeogeography, Palaeoclimatology, Palaeoecology, v. 252, p. 328–346.

Algeo, T.J., Henderson, C.M., Tong, J., Feng, Q., Yin, H., and Tyson, R. V., 2013, Plankton and productivity during the Permian-Triassic boundary crisis: An analysis of organic carbon fluxes: Global and Planetary Change, v. 105, p. 52–67, doi: 10.1016/j.gloplacha.2012.02.008.

Bhargava, O.N., Krystyn, L., Balini, M., Lein, R., and Nicora, A., 2004, Revised litho-and sequence stratigraphy of the Spiti Triassic: Albertiana, v. 30, p. 21–39.

Brühwiler, T., Bucher, H., and Goudemand, N., 2010, Smithian (Early Triassic) ammonoids from Tulong, South Tibet: Geobios, v. 43, p. 403–431.

Brühwiler, T., Goudemand, N., Galfetti, T., Bucher, H., Baud, A., Ware, D., Hermann, E., Hochuli, P.A., and Martini, R., 2009, The Lower Triassic sedimentary and

carbon isotope records from Tulong (South Tibet) and their significance for Tethyan palaeoceanography: Sedimentary Geology, v. 222, p. 314–332, doi: 10.1016/j.sedgeo.2009.10.003.

Chen, Z.Q., Yang, H., Luo, M., Benton, M.J., Kaiho, K., Zhao, L., Huang, Y., Zhang, K., Fang, Y., Jiang, H., Qiu, H., Li, Y., Tu, C., Shi, L., et al., 2015, Complete biotic and sedimentary records of the Permian-Triassic transition from Meishan section, South China: Ecologically assessing mass extinction and its aftermath: Earth-Science Reviews, v. 149, p. 67–107, doi: 10.1016/j.earscirev.2014.10.005.

Eltom, H.A., Abdullatif, O.M., and Babalola, L.O., 2018, The elemental geochemistry of Lower Triassic shallow-marine carbonates from central Saudi Arabia: Implications for redox conditions in the immediate aftermath of the latest Permian mass extinction: Journal of African Earth Sciences, v. 139, p. 283–306, doi: 10.1016/j.jafrearsci.2017.12.020.

Garzanti, E., Nicora, A., and Rettori, R., 1998, Permo-Triassic boundary and Lower to Middle Triassic in South Tibet: Journal of Asian Earth Sciences, v. 16, p. 143–157, doi: 10.1016/S0743-9547(98)00007-5.

Ghosh, N., Basu, A.R., Bhargava, O.N., Shukla, U.K., Ghatak, A., Garzione, C.N., and Ahluwalia, A.D., 2016, Catastrophic environmental transition at the Permian-Triassic Neo-Tethyan margin of Gondwanaland: Geochemical, isotopic and sedimentological evidence in the Spiti Valley, India: Gondwana Research, v. 34, p. 324–345.

Haas, J., Demény, A., Hips, K., Zajzon, N., Weiszburg, T.G., Sudar, M., and Pálfy, J.,

2007, Biotic and environmental changes in the Permian–Triassic boundary interval recorded on a western Tethyan ramp in the Bükk Mountains, Hungary: Global & Planetary Change, v. 55, p. 136–154.

Henderson, C.M., 2011, Biostratigraphic correlation and shale fabric of Lower Triassic strata, East-Central British Columbia (NTS 093I, O, P): Geoscience BC Summary of Activities, p. 223–228.

Horacek, M., Koike, T., and Richoz, S., 2009, Lower Triassic $\delta^{13}C$ isotope curve from shallow-marine carbonates in Japan, Panthalassa realm: Confirmation of the Tethys $\delta^{13}C$ curve: Journal of Asian Earth Sciences, v. 36, p. 481–490.

Horacek, M., Richoz, S., Brandner, R., Krystyn, L., and Spötl, C., 2007, Evidence for recurrent changes in Lower Triassic oceanic circulation of the Tethys: The $\delta^{13}C$ record from marine sections in Iran: Palaeogeography, Palaeoclimatology, Palaeoecology, v. 252, p. 355–369, doi: 10.1016/j.palaeo.2006.11.052.

Krystyn, L., Richoz, S., and Bhargava, O.N., 2007, The Induan-Olenekian boundary (IOB) in Mud - an update of the candidate GSSP section M04: Albertiana,.

Li, S., Tong, J., Liu, K., Wang, F., and Huo, Y., 2007, The Lower Triassic cyclic deposition in Chaohu, Anhui Province, China: Palaeogeography, Palaeoclimatology, Palaeoecology, v. 252, p. 188–199, doi: 10.1016/j.palaeo.2006.11.043.

Loope, G.R., Kump, L.R., and Arthur, M.A., 2013, Shallow water redox conditions from the Permian–Triassic boundary microbialite: The rare earth element and iodine geochemistry of carbonates from Turkey and South China: Chemical

Geology, v. 351, p. 195–208.

Luo, G., Wang, Y., Yang, H., Algeo, T.J., Kump, L.R., Huang, J., and Xie, S., 2011, Stepwise and large-magnitude negative shift in $\delta^{13}$Ccarb preceded the main marine mass extinction of the Permian–Triassic crisis interval: Palaeogeography Palaeoclimatology Palaeoecology, v. 299, p. 70–82.

Orchard, M.J., and Krystyn, L., 1998, Conodonts of the lowermost Triassic of Spiti, and new zonation based on Neogondolella successions: Rivista Italiana Di Paleontologia E Stratigrafia, v. 104, p. 341–368.

Sano, H., Onoue, T., Orchard, M.J., and Martini, R., 2012, Early Triassic peritidal carbonate sedimentation on a Panthalassan seamount: the Jesmond succession, Cache Creek Terrane, British Columbia, Canada: Facies, v. 58, p. 113–130.

Shen, S.Z., Cao, C.Q., Henderson, C.M., Wang, X.D., Shi, G.R., Wang, Y., and Wang, W., 2006, End-Permian mass extinction pattern in the northern peri-Gondwanan region: Palaeoworld, v. 15, p. 3–30, doi: 10.1016/j.palwor.2006.03.005.

Shen, S., Cao, C.Q., Shi, G.R., Wang, X.D., and Mei, S.L., 2003, Lopingian (Late Permian) stratigraphy, sedimentation and palaeobiogeography in southern Tibet: Newsletters on Stratigraphy, v. 39, p. 157–179, doi: 10.1127/nos/39/2003/157.

Tian, L., Tong, J.N., Sun, D.Y., Xiong, Y.L., Wang, C.G., Song, H.J., Song, H.Y., and Huang, Y.F., 2014, The microfacies and sedimentary responses to the mass extinction during the Permian-Triassic transition at Yangou Section, Jiangxi Province, South China: Science China Earth Sciences, v. 57, p. 2195–2207, doi: 10.1007/s11430-014-4869-5.

Tobia, F.H., and Aqrawi, A.M., 2016, Geochemistry of rare earth elements in carbonate rocks of the Mirga Mir Formation (Lower Triassic), Kurdistan Region, Iraq: Arabian Journal of Geosciences, v. 9, p. 259.

Wang, L., Wignall, P.B., Sun, Y., Yan, C., Zhang, Z., and Lai, X., 2017, New Permian-Triassic conodont data from Selong (Tibet) and the youngest occurrence of Vjalovognathus: Journal of Asian Earth Sciences, v. 146, p. 152–167, doi: 10.1016/j.jseaes.2017.05.014.

Wardlaw, B.R., Nestell, M.K., Nestell, G.P., Ellwood, B.B., and Lan, L.T.P., 2015, Conodont biostratigraphy of the Permian-Triassic boundary sequence at Lung Cam, Vietnam: Micropaleontology, v. 61, p. 313–334.

Wignall, P.B., and Hallam, A., 1993, Griesbachian (Earliest Triassic) palaeoenvironmental changes in the Salt Range, Pakistan and southeast China and their bearing on the Permo-Triassic mass extinction: Palaeogeography, Palaeoclimatology, Palaeoecology, v. 102, p. 215–237, doi: 10.1016/0031-0182(93)90068-t.

Wignall, P.B., and Twitchett, R.J., 2002, Extent, duration, and nature of the Permian-Triassic superanoxic event: Geological Society of America Special Paper, v. 356, p. 395–413, doi: 10.1130/0-8137-2356-6.395.

Wignall, P.B., and Newton, R., 2003, Contrasting deep-water records from the Upper Permian and Lower Triassic of South Tibet and British Columbia: Evidence for a diachronous mass extinction: Palaios, v. 18, p. 153–167.

Xie, S., Pancost, R.D., Huang, J., Wignall, P.B., Yu, J., Tang, X., Chen, L., Huang, X.,

and Lai, X., 2007, Changes in the global carbon cycle occurred as two episodes during the Permian-Triassic crisis: Geology, v. 35, p. 1083–1086, doi: 10.1130/G24224A.1.

Yin, H., Jiang, H., Xia, W., Feng, Q., Zhang, N., and Shen, J., 2014, The end-Permian regression in South China and its implication on mass extinction: Earth-Science Reviews, v. 137, p. 19–33.

Yin, H., Zhang, K., Tong, J., and Yang, Z., 2001, The global stratotype section and point (GSSP) of the Permian-Triassic boundary: China Basic Science, v. 24, p. 102–114.

Zhao, L., Orchard, M.J., Tong, J., Sun, Z., Zuo, J., Zhang, S., and Yun, A., 2007, Lower Triassic conodont sequence in Chaohu, Anhui Province, China and its global correlation: Palaeogeography Palaeoclimatology Palaeoecology, v. 252, p. 24–38, doi: 10.1016/j.palaeo.2006.11.032.